Integration of Apocarotenoid Profile and Expression Pattern of *Carotenoid Cleavage Dioxygenases* during Mycorrhization in Rice

Cristina Votta[1*], Jian You Wang[2*], Nicola Cavallini[3], Francesco Savorani[3], Kit Xi Liew[2], Luisa Lanfranco[1], Salim Al-Babili[2,4#], Valentina Fiorilli[1#]

1 Department of Life Sciences and Systems Biology, University of Torino, Viale Mattioli 25, Torino 10125, Italy.

2 The BioActives Lab, Center for Desert Agriculture, King Abdullah University of Science and Technology, Thuwal, 23955-6900, Saudi Arabia

3 Institute of Chemistry, Department of Applied Science and Technology (DISAT), Polytechnic University of Turin, Corso Duca degli Abruzzi 24, 10129 Torino, Italy

4 The Plant Science Program, Biological and Environmental Science and Engineering Division, King Abdullah University of Science and Technology, Thuwal, 23955-6900, Saudi Arabia

* These authors contributed equally to this work

Correspondence: valentina.fiorilli@unito.it, salim.babili@kaust.edu.sa

valentina.fiorilli@unito.it (https://orcid.org/0000-0001-9805-1559)

salim.babili@kaust.edu.sa (https://orcid.org/0000-0003-4823-2882)

Number of tables: 1

Number of figures: 5

Word count: 4661 words

Supplementary data figures: 7

Supplementary data tables: 1

Running title: Apocarotenoid profile and *CCD* expression in AM symbiosis

27 **Highlight**

28 Our study presents the profiles of *CCD* gene expression and apocarotenoids across different stages
29 of AM symbiosis and Pi supply conditions and reveals novel AM markers at both local and
30 systemic levels.

31 ## Abstract

32 Carotenoids are susceptible to degrading processes initiated by oxidative cleavage reactions
33 mediated by Carotenoid Cleavage Dioxygenases that break their backbone, leading to products
34 called apocarotenoids. These carotenoid-derived metabolites include the phytohormones abscisic
35 acid and strigolactones, and different signaling molecules and growth regulators, which are utilized
36 by plants to coordinate many aspects of their life. Several apocarotenoids have been recruited for
37 the communication between plants and arbuscular mycorrhizal (AM) fungi and as regulators of the
38 establishment of AM symbiosis. However, our knowledge on their biosynthetic pathways and the
39 regulation of their pattern during AM symbiosis is still limited. In this study, we generated a
40 qualitative and quantitative profile of apocarotenoids in roots and shoots of rice plants exposed to
41 high/low phosphate concentrations, and upon AM symbiosis in a time course experiment covering
42 different stages of growth and AM development. To get deeper insights in the biology of
43 apocarotenoids during this plant-fungal symbiosis, we complemented the metabolic profiles by
44 determining the expression pattern of *CCD* genes, taking advantage of chemometric tools. This
45 analysis revealed the specific profiles of *CCD* genes and apocarotenoids across different stages of
46 AM symbiosis and phosphate supply conditions, identifying novel markers at both local and
47 systemic levels.

48 **Keywords**

49 Apocarotenoids, arbuscular mycorrhizal symbiosis, *Carotenoid Cleavage Dioxygenases*,
50 chemometric tools, rice, strigolactone, zaxinone.

51

Introduction

Carotenoids represent are a widespread class of tetraterpene (C_{40}) lipophilic pigments, synthesized by all photosynthetic organisms, including bacteria, algae, and plants, and by numerous non-photosynthetic microorganisms (Moise *et al.*, 2014; Nisar *et al.*, 2015). In plants, carotenoids are essential constituents of the photosynthetic apparatus where they act as photo-protective pigments and take part in the light-harvesting process. Further, these pigments have ecological functions, providing flowers and fruits with specific colors and flavors that attract insects and other animals or act as a repellent for pathogens and pests (Cazzonelli, 2011).

The carotenoid structure, rich in electrons and conjugated double bonds, makes them susceptible to oxidation, which causes the breakage of their backbone and leads to a wide range of metabolites called apocarotenoids (Moreno *et al.*, 2021). These compounds can be generated by non-enzymatic processes that are triggered by reactive oxygen species (ROS) (Harrison and Bugg, 2014; Ahrazem *et al.*, 2016) or by the action of a ubiquitous family of non-heme iron enzymes, Carotenoid Cleavage Dioxygenases (CCDs) (Jia *et al.*, 2018).

The genome of the model plant *Arabidopsis thaliana* encodes nine members of the CCD family, including five *NINE-CIS-EPOXY CAROTENOID CLEAVAGE DIOXYGENASES* (*NCED2, NCED3, NCED5, NCED6,* and *NCED9*) and four *CCD*s (*CCD1, CCD4, CCD7,* and *CCD8*) (Tan *et al.*, 2003; Sui *et al.*, 2013). In short, NCEDs catalyze the first step in abscisic acid (ABA, C_{15}) biosynthesis, i.e. the cleavage of 9-*cis*-violaxanthin or 9'-*cis*-neoxanthin into the ABA precursor xanthoxin (Nambara and Marion-Poll, 2005; Ahrazem *et al.*, 2016). CCD1 cleaves several carotenoids and apocarotenoids at different positions along their hydrocarbon backbone (Schwartz *et al.*, 2001; Vogel *et al.*, 2008; Ilg *et al.*, 2009, 2014; Jia *et al.*, 2018) generating volatiles, such as β-ionone and geranylacetone, and a diverse set of dialdehydes in fruits and flowers of many plant species (Moreno *et al.*, 2021). CCD4 enzymes are known to produce apocarotenoid-derived pigments, flavors, and aromas *in planta*, but their cleavage specificities differ considerably from those of CCD1 enzymes (Schwartz *et al.*, 2001; Auldridge *et al.*, 2006; Ilg *et al.*, 2009; McQuinn *et al.*, 2015; Hou *et al.*, 2016). In plants, two different forms of CCD4 are present (Huang *et al.*, 2009; Mi and Al-Babili, 2019): the first one is common in *Citrus* and is involved in forming the pigment citraurin (3-hydroxy-β-apo-8'-carotenal, C_{30}) formation by catalyzing a single cleavage reaction at the 7',8' double bond of zeaxanthin and β-cryptoxanthin (Ma *et al.*, 2013; Rodrigo *et al.*, 2013), while the other type cleaves bicyclic all-*trans*-carotenoids at the C9, C10 or C9', C10' double bond leading to apo-10'-carotenoids (C_{27}) and the corresponding C_{13} cyclohexenones, e.g. β-ionone (Bruno *et al.*, 2015, 2016). Recently, a Gardinia CCD4 enzyme (GjCCD4a) was shown to catalyze

85   sequential cleavage of β-carotene and zeaxanthin at the C7, C8 and C8', C9' leading to crocetin

86   dialdehyde, the precursor of the saffron pigment crocins, and to cyclocitral and 3-hydroxy-

87   cyclocitral, respectively (Zheng et al., 2022).

88   The two CCD-subfamilies CCD7 and CCD8 are involved in the biosynthesis of the plant hormone

89   strigolactones (SLs) (Wang *et al.*, 2021). CCD7 cleaves 9-*cis*-β-carotene (C_{40}), yielding β-ionone

90   and 9-*cis*-β-apo-10'-carotenal (C_{27}); while CCD8 converts 9-*cis*-apo-10'-carotenal (C_{27}) *via* a

91   combination of different reactions into the SL precursor carlactone (C_{19}) and ω-OH-(4-CH3)

92   heptanal (C_8) (Alder *et al.*, 2012; Chen *et al.*, 2022). In addition, CCD7 may also catalyze the initial

93   9,10 cleavage required for mycorradicin synthesis (Floss *et al.*, 2008).

94   A recent survey on plant genomes identified the Zaxinone Synthase (ZAS) as a representative for a

95   further CCD subfamily, which is conserved in most land plants but missing in non-mycorrhizal

96   species, i.e., *A. thaliana* (Fiorilli *et al.*, 2019; Wang *et al.*, 2019). *In vitro*, this enzyme cleaves the

97   apocarotenoid 3-OH-β-apo-10'-carotenal (C_{27}) at the C13-C14 double bond, generating zaxinone, a

98   C_{18}-ketone (3-OH-β-apo-13-carotenone) that acts as a growth regulator, and an unstable C_9-

99   dialdehyde (Wang *et al.*, 2019). Loss-of-function *zas* mutant showed a decreased zaxinone content

100   in roots, reduced shoot, and root growth, and a higher SL level compared to wild-type rice plants

101   (Wang *et al.*, 2019). Phylogenetic analyses revealed that the rice genome encodes three *OsZAS*

102   homologs, named *OsZAS1b*, *OsZAS1c*, and *OsZAS2* (Ablazov *et al.*, 2023). Intriguingly, although

103   *OsZAS2* is placed in a clade different from that of ZAS, it catalyzes the same reaction, and both

104   enzymes contribute to zaxinone production in rice (Ablazov *et al.*, 2023).

105   Apocarotenoids play several roles in plants, from regulating root and shoot developmental

106   processes to coordinating plant responses to abiotic and biotic stress (Moreno *et al.*, 2021). They are

107   also emerging signaling molecules implicated in plant-microbe interactions, including the

108   arbuscular mycorrhizal (AM) symbiosis (Fiorilli *et al.*, 2019). The AM symbiosis is one of the most

109   ancient and widespread associations, formed by approximately 70% of land plants (Wang and Qiu,

110   2006; Brundrett, 2009), including major crops, with soil fungi belonging to the Glomeromycotina

111   group (Spatafora *et al.*, 2016). In this symbiosis, the fungus facilitates the plant uptake of minerals,

112   predominantly phosphorus (P) and nitrogen (N) (Smith *et al.*, 2011), and the tolerance to biotic and

113   abiotic stress (Pozo *et al.*, 2010; Chen *et al.*, 2018). Meanwhile, the plant provides the fungus with

114   fixed organic carbon. The establishment of the AM symbiosis includes several steps, starting with

115   partner recognition *via* diffusible molecules that activate the common symbiosis signaling pathway

116   (MacLean *et al.*, 2017) and trigger the development of fungus adhesion structures, called

117   hyphopodia, on the root epidermis. These structures permit the fungus to enter the host root tissues

118   and proliferate within cells or intracellularly (Bonfante and Requena, 2011; Nadal and Paszkowski,

4

119   2013). Finally, fungal hyphae invade the inner cortical layers, penetrate single cells and form highly
120   branched tree-shaped hyphal structures, the arbuscules, where nutrient exchanges occur (Harrison,
121   2012; Gutjahr and Parniske, 2013). During these stages, the plant controls fungal expansion and
122   symbiotic functions, by activating a series of cellular, metabolic, and physiological changes
123   (Gutjahr, 2014; Carbonnel and Gutjahr, 2014). Among the environmental factors that regulate AM
124   colonization, phosphate (Pi) availability is certainly one of the most crucial ones (Smith *et al.*,
125   2011; Richardson *et al.*, 2011). It has been recently shown that a complex gene network centered on
126   the plant Pi starvation response actively supervises AM fungal development in roots, acting at the
127   local and systemic level (Shi *et al.*, 2021; Das *et al.*, 2022). Pi starvation also induces SL
128   biosynthesis and release (Yoneyama *et al.*, 2007; Wang *et al.*, 2017, 2022), while high Pi levels
129   repress the expression of genes involved in the biosynthesis of carotenoids and SLs in root
130   (Carbonnel and Gutjahr, 2014; Haider *et al*., 2023). SLs are the best-known plant molecules active
131   in the pre-symbiotic interaction with AM fungi. In Pi-starved plants, SLs are produced by roots and
132   exported to the rhizosphere, which directly stimulates AM fungal metabolism, gene expression, and
133   hyphal branching, supporting the development of this symbiosis (Waters *et al.*, 2017; Müller and
134   Harrison, 2019). Notably, (Volpe *et al.*) recently showed that SL biosynthesis is stimulated by
135   chito-oligosaccharides released by AM fungi.

136   Studies of the last decade highlighted that other apocarotenoid compounds are involved in the AM
137   symbiosis (Fiorilli *et al.*, 2019 and reference therein), including the plant hormone ABA that is
138   known for coordinating plant's response to biotic and abiotic stress factors (Felemban *et al.*, 2019;
139   Moreno *et al.*, 2021). ABA has been reported to be involved in mycorrhizal colonization in
140   different host plants, probably through synergistic and antagonistic interactions with other
141   hormones (Herrera-Medina *et al.*, 2007; Martín-Rodríguez *et al.*, 2011; Charpentier *et al.*, 2014).
142   Specifically, a positive correlation between ABA levels and SL biosynthesis was observed,
143   suggesting that ABA and SLs collaborate to influence the outcome of the symbiosis (López-Ráez *et*
144   *al.*, 2010). In contrast, ABA controls the normal development of arbuscules by inhibiting ethylene
145   production (Martín-Rodríguez *et al.*, 2011) and acts as an antagonist of gibberellins (GA) by down-
146   regulating their biosynthesis and promoting their catabolism (Floss *et al.*, 2013; Martín-Rodríguez
147   *et al.*, 2016).

148   Blumenols (C_{13}) and mycorradicin (C_{14}) are further apocarotenoids associated with AM symbiotic
149   establishment and maintenance (Walter *et al.*, 2007; Floß *et al.*, 2008; Floss *et al.*, 2008; Fiorilli *et*
150   *al.*, 2019) and described as a signature for AM symbiosis because of their being specifically
151   accumulated in mycorrhizal plants (Walter *et al.*, 2007; Hill *et al.*, 2018; Moreno *et al.*, 2021).
152   Mycorradicins cause typical yellow/orange pigmentation of roots, which enabled their identification

153 (Scannerini and Bonfante-Fasolo, 1977; Klingner *et al.*, 1995; Floss *et al.*, 2008). Blumenols are

154 accumulated in roots and shoots of host plants in direct correlation with the fungal colonization rate

155 (Klingner *et al.*, 1995; Maier *et al.*, 1997; Walter *et al.*, 2000; Fester *et al.*, 2002; Strack and Fester,

156 2006). Even if their biological role has not yet been clarified, blumenols have been proposed as

157 foliar markers that allow rapid detection of AM symbiosis and screening of functional AM

158 associations (Walter *et al.*, 2010; Wang *et al.*, 2018). Finally, zaxinone, a recently discovered

159 apocarotenoid growth regulator (Wang *et al.*, 2019; Ablazov *et al.*, 2020) is also involved in AM

160 symbiosis and acts as a component of a regulatory network that includes SLs, as demonstrated by

161 that the impact of the rice gene encoding Zaxinone Synthase (*OsZAS*) on the extent of AM

162 colonization SLs (Votta *et al.*, 2022).

163 In the current study, we further explored the involvement of apocarotenoids in the AM symbiosis.

164 For this purpose, we generated a qualitative and quantitative profile of apocarotenoids in roots and

165 shoots of rice plants exposed to high/low Pi concentrations (+Pi and -Pi) and upon AM symbiosis in

166 a time course experiment covering different stages of growth and AM development. We

167 complemented the metabolic profiles by characterizing the expression pattern of *CCD* genes and

168 took advantage of chemometric tools to get deeper insights in the biology of apocarotenoids during

169 this plant-fungal symbiosis.

Materials and methods

171 **Plant and fungal materials.** Rice seeds of wild-type (WT) (cv. Nipponbare) were germinated in

172 pots containing sand and incubated for 10 days in a growth chamber under 14 h light (23 °C)/10 h

173 dark (21 °C). A set of plants (MYC) was inoculated with *Funneliformis mosseae* (BEG 12,

174 MycAgroLab, France). The fungal inoculum (15%) was mixed with sterile quartz sand and used for

175 colonization. A group of non-mycorrhizal plants (no-myc -Pi) was also set up. These two groups of

176 plants (MYC and no-myc -Pi) were watered with a modified Long-Ashton (LA) solution containing

177 3.2 μM $Na_2HPO_4 \cdot 12H_2O$ (low Pi) and grown in a growth chamber under 14 h light (24 °C)/10 h

178 dark (20 °C) regime. Another group of no-myc WT plants was watered with a LA containing 500

179 μM $Na_2HPO_4 \cdot 12 H_2O$ (+Pi) and grown in the same condition described above; these plants were

180 considered the no-myc + Pi samples. Plants for the three different conditions (MYC, no-myc -Pi,

181 no-myc +Pi) were collected at three time points: 7 days post-inoculation (dpi), 21 dpi, and 35 dpi.

182 For the molecular and metabolites analyses, roots and shoots samples were harvested and

183 immediately frozen in liquid nitrogen and stored at -80° C.

184   **Qualitative and quantitative profiling of plant apocarotenoids (APOs).** Following the method

185   used by Mi *et al.* (2018), about 20 mg lyophilized root and shoot tissue powder was spiked with

186   Internal Standards (IS) mixture (2 ng each standard) and extracted with 2 mL of methanol

187   containing 0.1% butylated hydroxytoluene (BHT) in an ultrasound bath (Branson 3510 ultrasonic

188   bath) for 15 min, followed by the centrifugation. The supernatant was collected, and the pellet was

189   re-extracted with 2 mL of the same solvent. The two supernatants were then combined and dried

190   under vacuum. The residue was re-dissolved in 150 µL of acetonitrile and filtered through a 0.22

191   mm filter for LC-MS analysis.

192   Analysis of apocarotenoids was performed on a Dionex Ultimate 3000 UHPLC system coupled

193   with a Q-Orbitrap-MS (Q-Exactive plus MS, Thermo Scientific) with a heated electrospray

194   ionization source. Chromatographic separation was carried out on an ACQUITY UPLC BEH C_{18}

195   column (100 x 2.1mm, 1.7 µm) with a UPLC BEH C18 guard column (5 x 2.1mm, 1.7 mm)

196   maintained at 35° C. UHPLC conditions including mobile phases and gradients were optimized

197   based on the separation of APOs and the time needed for sample analysis. APO isomers were

198   identified by MS/MS fragmentation.

199   The quantification of APOs was calculated as follows: Amount [target APO] = Area [target

200   APO]/Area [spiked IS] x Amount [spiked IS]/ mg materials. The experiment was repeated twice

201   with equivalent results.

202   **Gene expression analysis.** Total RNA was extracted from WT rice roots using the Qiagen Plant

203   RNeasy Kit according to the manufacturer's instructions (Qiagen, Hilden; Germany). Following the

204   producer's directives, samples were treated with TURBO™ DNase (Thermofischer). The RNA

205   samples were routinely checked for DNA contamination through PCR analysis. Single-strand

206   cDNA was synthesized from 1 µg of total RNA using Super-Script II (Invitrogen) according to the

207   instructions in the user manual. Quantitative RT-PCR (qRT-PCR) was performed using a Rotor-

208   Gene Q 5plex HRM Platform (Qiagen). All reactions were performed on at least three biological

209   and three technical replicates. Baseline range and take-off values were automatically calculated

210   using Rotor-Gene Q 5plex software. The transcript level of genes listed in **Supplemental Table 1**

211   was normalized using *OsRubQ1* housekeeping gene (Güimil *et al.*, 2005). Only take-off values

212   leading to a Ct mean with a standard deviation below 0.5 were considered. The experiment was

213   repeated twice with equivalent results.

214   **Statistics and reproducibility**. Both experiments (plant apocarotenoid quantification and CCD

215   gene expression analysis) were performed with at least three biological replicates each. Statistical

216   tests were carried out through One-way analysis of variance (One-way ANOVA) and Tukey's *post*

217   *hoc* test, using a probability level of P<0.05. All statistical elaborations were performed using

218   PAST statistical package version 4 (Hammer *et al.* 2001).

219   **Data quality assessment and preprocessing.** Gene and apocarotenoid datasets were inspected to

220   spot potential extreme samples or outliers. Different preprocessing approaches were tested,

221   including autoscaling (i.e., column scaling to unit variance, followed by mean centering) and

222   normalization to a unit area (i.e., the normalization factor of each sample was computed from its

223   "area under the curve") followed by mean centering. Based on the ease of interpretation, we

224   selected the following preprocessing: mean centering alone for the apocarotenoids dataset, and

225   autoscale for the gene dataset. All modeling results were therefore obtained from the two datasets

226   preprocessed as such. With respect to the analysis with the low-level data fusion approach (i.e.,

227   combining the two datasets into an individual one), a different sequence tailored to the issue of

228   obtaining an equal representation of the two datasets was used, as described in the dedicated

229   paragraph further in the section Data fusion approach.

230   **Exploratory analysis.** All chemometric models reported in this work are "exploratory", meaning

231   that they describe the phenomena and natural groupings captured in the data, in an unsupervised

232   manner (Li Vigni *et al.* 2013). To this aim, Principal Component Analysis (PCA) (Bro & K. Smilde

233   2014) was employed. This technique is employed to capture, in sequence, the largest sources of

234   variability by defining new variables (the so-called "Principal Components", PCs), which are

235   summaries of the different pieces of information contained in the data. This "summarized" version

236   of the information can be inspected with the scores and loadings plots, which are scatter plots

237   obtained by plotting pairs (and sometimes triplets) of PCs. The scores plot allows inspecting the

238   relationships among the samples and thus spotting possible groupings and tendencies or patterns of

239   interest, while the loadings plot allows inspecting the relationships among the variables of the data,

240   providing at the same time an interpretation of the scores plot. In our study, individual

241   apocarotenoids and genes were identified by their systematic names and inspected in PCA as the

242   samples. At the same time, the variables of the datasets were the combinations of three-time points

243   (7, 21, and 35 dpi) and three conditions (MYC, no-myc -Pi, no-myc +Pi) for a total of nine

244   combinations.

245   **Data fusion approach**. For this study we also tested a low-level data fusion approach (Borràs *et al.*

246   2015) to combine and jointly explore the information of the apocarotenoids and genes datasets. In

247   practice, the apocarotenoids dataset was joined with the gene dataset in the sample direction so that

248 the nine variables (combinations of time points and conditions) were coherent between the two

249 datasets, i.e., the information described by each column had to be the same in both datasets.

250 We performed the following data preprocessing and fusion sequence: (i) standard deviation scaling

251 for each APO/gene quantification, (ii) fusion of the two data tables, (iii) group scale to give the two

252 data tables the same importance (i.e., each dataset accounts for 50 % of the total variance of the

253 resulting fused dataset), (iv) mean center. The new fused data table was then modelled with PCA,

254 with the apocarotenoids and the genes as the samples (rows) and the combinations of time points

255 and treatments as the variables (columns) (**Supplementary Fig.S1**).

Results

CCD gene expression pattern during AM symbiosis

258 We determined the transcript level of a set of *CCD* gene, including *CCD1, CCD4a, CCD4b, CCD7,*

259 *CCD8, ZAS1, ZAS1b, ZAS1c,* and *ZAS2*, in mycorrhizal plants grown at low Pi (3.2 μM) and in non-

260 mycorrhizal plants grown at low (3.2 μM) or high Pi (500 μM). We measured the transcript levels

261 at early (7 dpi), middle (21 dpi), and late (35 dpi) stage of AM symbiosis development

262 (**Supplementary Fig. S2**). To assess the statistically significant differences, all samples were

263 referred to the -Pi condition within each time point. As shown in the heatmap (**Fig. 1A**) referred to

264 roots, *CCD1, CCD4a*, and *CCD4b* transcript level increased at 21 dpi in the +Pi condition

265 compared to -Pi and MYC ones. Concerning the SL biosynthetic genes, we observed an induction

266 of *CCD7* in MYC roots at the middle and late stage (21, 35 dpi), while *CCD8* was induced at 7 dpi

267 under the MYC condition, and, as expected, down-regulated under +Pi condition in the later time

268 points (at 21 and 35 dpi) (López-Ráez *et al.*, 2008; Yoneyama *et al.*, 2013). At the middle stage

269 (21dpi), *ZAS1* showed an up-regulation in MYC samples and a down-regulation under +Pi. The

270 *ZAS1* homolog, *ZAS1b* was upregulated at 21 dpi in MYC and +Pi roots, while we detected a down-

271 regulation in MYC roots during the later stage. By contrast, *ZAS1c* was up-regulated at 35 dpi in

272 MYC roots. Finally, *ZAS2* expression level increased at 21 dpi in +Pi. **Supplementary Fig. S3A.**

273 *CCDs* gene expression pattern in shoots (**Fig. 1B, Supplementary Fig. S3B**) displayed several

274 differences compared to roots. We detected induction of *CCD1* at 21 dpi in the +Pi condition, while

275 its expression decreased in the MYC condition at 21 and 35 dpi. *CCD4a* showed an expression

276 profile similar to *CCD1*. By contrast, *CCD4b* displayed an opposite trend compared to *CCD4a* with

277 an up-regulation at 35 dpi in the MYC condition. Moreover, *CCD4b* displayed an up-regulation at 7

278 dpi in the +Pi condition. We did not observe significant changes in the *CCD7* expression level

279 across all conditions or time points, while *CCD8* transcript level was up-regulated at 7 dpi (MYC

280   and +Pi conditions) and down-regulated in the later stages (21 and 35 dpi) in shoots of plants grown

281   in +Pi and at 35 dpi in shoots of MYC plants. *ZAS1* displayed a down-regulation trend in all time

282   points and conditions considered, with a statistically significant difference in mycorrhizal samples

283   at 7 dpi. *ZAS1b*, and *ZAS1c*, showed an up-regulation in leaves of the MYC plant at the first time

284   point (7 dpi) and 21 dpi upon +Pi. Lastly, *ZAS2* was barely detected in the shoot of plant growth at

285   low Pi, while it showed an up-regulation at 21 dpi in MYC and +Pi conditions and a down-

286   regulation in +Pi at 35 dpi.

287   We used PCA to assess the samples' natural grouping and clustering tendencies under the different

288   growth conditions (MYC, -Pi, and +P) at the three-time points analyzed. The loading plot of **Fig.**

289   **2A** describes the influence of the measured variables on the samples' distribution shown in the

290   scores plot of **Fig. 2B** that provides insights into this distribution.

291   In our study, the PCA model was obtained from the expression level of the set of genes analyzed in

292   all samples, in which PC1 explained 43.88% (related to the gene expression level) and PC2

293   explained 22.23% (related to the plant developmental stage) of the total variance (**Supplementary**

294   **Fig. S4**). PC1 and PC2 models highlight that in all growth conditions the middle developmental

295   stage (21 dpi) presented a different *CCD* expression pattern compared to early and late stages. We

296   selected the model with 5 PCs, since PC3 (9.90%) and PC5 (5.53%) provided notable information

297   related to the growth conditions, as shown in the loading plot (**Fig. 2A**), while the scores plot (**Fig.**

298   **2B**) displayed a clear separation between the plant organs: roots and shoots. More in detail, **Fig. 2B**

299   showed that *CCD1* and *CCD7* expression in roots was mainly influenced by Pi level, while that of

300   *CCD8* was affected by both Pi level and MYC condition. *CCD4a, ZAS1c,* and *ZAS1* expression was

301   more affected by the time point than by the Pi level. By contrast, the *CCD4b* and *ZAS2* expression

302   levels were mainly influenced by the Pi level.

303   Concerning the shoot, *CCD1, CCD4a, CCD4b,* and *ZAS2* were located in the plot area influenced

304   by the Pi level during the middle and late stages (21 and 35 dpi), while *CCD7* and *ZAS1c* fell in the

305   plot area related to the MYC condition.

Apocarotenoid profile

307   To profile non-hydroxylated and hydroxylated apocarotenoids (**Table 1**) in roots and shoots of rice

308   plants grown in high/low Pi concentration (+Pi and -Pi) and upon MYC condition, we used the

309   ultra-HPLC (UHPLC)-mass spectrometry (MS)-based approach to get insight into the

310   apocarotenoid compositions (Mi *et al.*, 2018). To simplify this analysis, the statistically significant

311   differences were referred to as the -Pi condition within each time point. The results showed a

312   substantial difference between roots and shoots in the apocarotenoid quantification and distribution,

313   in analogy to what has been observed in *CCDs* gene expression data.

314   With respect to roots (**Fig. 3A, Supplementary Fig. S5A**), we observed an increment of the content

315   of Apo9 (β-ionone), Apo10, and their hydroxylated forms (OH-Apo9 and OH-Apo10) in MYC

316   condition at 21 dpi and 35 dpi. In addition, Apo10 showed a higher accumulation in MYC roots and

317   upon +Pi at 7 dpi. Likewise, at the same time point, the Apo11 level increased in the MYC

318   condition, while it decreased during the middle stage (21 dpi), contrary to its hydroxylated forms

319   (OH-Apo 11 and OH-Apo 11-iso) that showed a strong accumulation. Moreover, at 35 dpi, all the

320   β-apo-11-carotenoids (C_{15}) showed a statistically significant decrease upon +Pi. Apo12 and Apo14

321   displayed the same pattern at 35 dpi: both showed a higher accumulation in MYC and +Pi

322   compared to -Pi. By contrast, we observed an increase of Apo13 in MYC and +Pi conditions during

323   the early (7 dpi) and middle stages (21 dpi); its hydroxylated forms (OH-Apo13 and OH-Apo13-

324   iso) also displayed a higher content at 7 dpi in the +Pi condition and 21 dpi in the MYC root.

325   Moreover, at the later stage (35 dpi), OH-Apo13-iso showed a statistically significant higher and

326   lower content in MYC and +Pi roots respectively. Finally, Apo15 and Apo15-iso displayed a higher

327   level at 21 dpi in MYC and +Pi roots.

328   Concerning the shoot, the heatmap (**Fig. 3B**) showed that the non-hydroxylated apocarotenoids

329   (from Apo 8 to Apo 15) displayed an overall similar profile: a general decrease at 7 and 35 dpi in

330   +Pi condition compared to plants grown at -Pi, and an increase upon MYC and +Pi during the

331   middle stage (21 dpi). Notably, Apo9, Apo10, Apo11, Apo12, Apo13, Apo14 and its isomer

332   (Apo14-iso), and Apo15 levels decreased at 7 dpi in the +Pi condition. By contrast, at 21 dpi, Apo9,

333   Apo10, Apo11, Apo12, Apo13, and Apo15 content increased in MYC and +Pi conditions, while

334   Apo14 and its isomer showed an increment only for the MYC condition. At the later time point (35

335   dpi), we detected a decrease of Apo9, Apo12, and Apo14 e its isomer content in MYC plants.

336   The hydroxylated forms showed a profile similar to non-hydroxylated APO with an increased

337   content at 21 dpi in the +Pi condition, and a decreasing trend in the MYC condition at 35 dpi. In

338   detail, at 7 dpi, the OH-Apo11 isomer showed a statistically different increase in MYC condition.

339   Further, at 21 dpi, OH-Apo8, OH-Apo10, OH-Apo11 and its isomer, OH-Apo12, OH-Apo13, OH-

340   Apo15, and OH-Apo15 isomer strongly increase in +Pi. At the same time point, also OH-Apo11

341   isomer and OH-Apo13 levels increased in the MYC condition, while the OH-Apo10 content

342   decreased. At the later stage, OH-Apo10 and OH-Apo11 displayed an increased content at +Pi,

343   while OH-Apo13-iso accumulation decreased in the shoot of plants grown in MYC and +Pi

344   conditions (**Supplementary Fig. S5B**).

345 To highlight correlations in apocarotenoids distribution across different stages of plant
346 development, AM symbiosis and Pi levels, a PCA was employed. In the apocarotenoid database, no
347 outliers (i.e., samples with clearly inconsistent values and/or unexpected behaviors attributable to
348 errors of measurement or to data acquisition problems) were identified, even if three apocarotenoids
349 (OH-Apo10, Apo10, and Apo12) showed very high values across all time points and treatments
350 (**Supplementary Fig. S6**). To better model the information of the rest of the samples, these three
351 extreme samples were removed from the apocarotenoid dataset and projected at a later stage to
352 inspect their position in the final PCA model.
353 In the PCA model referred to apocarotenoids, PC1 explained 43.88% (related to apocarotenoid
354 quantification) and PC2 explained 22.23% (related to growth conditions) of the total variance
355 (**Supplementary Fig. S7**). PC1 and PC2 models highlighted the apocarotenoids strictly related to
356 MYC condition (OH-Apo9; Apo11; OH-Apo11; OH-Apo13iso). Further, we adopted the PCA
357 model PC2 combined with PC3, where PC3 explained 2.55% of the total variation, upon the
358 propensity of samples to regroup following the temporal trend described in the loading plot (**Fig.
359 4A**).
360 In the plot chart, at 7 dpi all the growth conditions were clustered in the same area. Here, the
361 majority of the analyzed shoot apocarotenoids (Apo9, Apo11, OH-Apo11 isomer, OH-Apo13, OH-
362 Apo13 isomer, and Apo15) were located, suggesting that their content was mainly influenced by the
363 growth time than by the growth condition.
364 The scores plot (**Fig. 4B**) displayed a clear separation between the apocarotenoids quantified in
365 roots or shoots. In-depth, in root OH-Apo9, OH-Apo11, Apo11, and OH-Apo13 isomer were
366 mainly influenced by mycorrhization in different time points (21 dpi and 35 dpi). Instead, APO14
367 seems to be dependent on the Pi level and MYC condition. However, in shoot OH-Apo9, OH-
368 Apo12, and OH-Apo15 were linked to the +Pi condition. OH-Apo8, the OH-Apo12 isomer, and the
369 OH-Apo15 isomer depended on the Pi level at the middle stage (21 dpi).

Data fusion

371 Finally, to combine and investigate the potential correlation between apocarotenoids and CCD
372 genes, we used a low-level data fusion approach (Borràs *et al.*, 2015) to combine the two datasets
373 into an individual fused one, also modelled with PCA.
374 In the resulting PCA model, considering genes expression and apocarotenoids profiles joined, PC1
375 explained 29.65% and PC2 explained 26.81% of the total variance (**Fig. 5A, Fig. 5B**). From the
376 loading plot (**Fig. 5A**) we observed the grouping of the samples interpretable by the temporal trend
377 (7, 21, and 35 dpi). As reported for the previous scores plots referred to individual categories (genes

12

378   and apocarotenoids), in **Figure 5B** we observed a clear separation between plant organs. In more

379   detail, genes and apocarotenoids in the left upper part of the scores plot (**Fig. 5B**) were more related

380   to the early stage (7 dpi). Here, we found mainly shoot apocarotenoids, *CCD8* expressed in both

381   root and shoot, and *ZAS1c* in the root. By contrast, the lower left part of the plot, clustered

382   exclusively apocarotenoids and genes (*CCD7* and *ZAS1*) modulated in the root, depended on the

383   MYC condition during the middle and later stages. In particular, Apo9 (β-ionone), Apo10, and their

384   hydroxylated forms (OH-Apo9 and OH-Apo10) were grouped in this plot area, suggesting their

385   possible involvement during the AM colonization process. Furthermore, in the same area, we

386   highlighted the association between *CCD7* and one of its cleavage products, Apo9 (β-ionone). In

387   addition, this group highlighted the correlation between *ZAS1*, responsible for the OH-Apo13

388   (zaxinone) synthesis, and its precursors (OH-Apo10 and OH-Apo12).

389   In the shoot, most of the *CCD* genes (*CCD1, CCD4a, CCD7, ZAS1b, ZAS1c*, and *ZAS2*) were

390   mainly influenced by the Pi level and by the growing time (21 dpi and 35 dpi) similarly to some

391   genes (*CCD1, CCD4a, CCD4b,* and *ZAS2*) in the root. Moreover, the right area of the plot clustered

392   the majority of shoot apocarotenoids. On the whole, apocarotenoids profiles in the shoot seem to be

393   more influenced by the time points (7, 21, 35 dpi) and Pi availability, while, in the root, most

394   apocarotenoids and genes were mainly influenced by mycorrhization.

Discussion

396   In recent years, plant apocarotenoids are emerging not only as carotenoid breakdown products but

397   as metabolites with active roles in regulating physiological and developmental processes and plant-

398   (a)biotic interactions (Zheng *et al.*, 2021). In particular, some apocarotenoids were associated with

399   the establishment and maintenance of AM symbiosis (Fiorilli *et al.*, 2019). Investigations over the

400   last decade indicate that beyond SLs, ABA, mycorradicins, and blumenols (Walter *et al.*, 2007;

401   Floss *et al.*, 2008; Hill *et al.*, 2018; Wang *et al.*, 2018; Fiorilli *et al.*, 2019), other apocarotenoids

402   may play a role in this mutualistic association. For example, zaxinone, generated by the activity of

403   the CCD subfamily Zaxinone Synthases, was shown to control the extent of AM root colonization

404   with a complex interplay with SLs (Votta *et al.*, 2022; Ablazov *et al.*, 2023). To further explore the

405   involvement of other apocarotenoids in the AM symbiosis in this work we developed a combined

406   approach: we profiled apocarotenoids in rice roots and shoots across a time course (7, 21, and 35

407   dpi) experiment of AM colonization by LC-MS (Mi *et al.*, 2018) and, in parallel, we monitored the

408   expression pattern of a set of CCD genes. To highlight genes and apocarotenoids more specifically

409   related to the AM association, we analyzed plants grown in low and high Pi conditions. Our results

410   show that the AM colonization, although confined to the root system, can trigger a systemic

13

411 response which is evident from the modulation of *CCDs* gene expression and apocarotenoid content

412 in rice shoots. The effect on epigeous organs exerted by AM root colonization has been already

413 described in other species (Fiorilli *et al.*, 2009, 2018; Zouari *et al.*, 2014). In addition, our analysis

414 indicates that both mycorrhization and Pi availability triggered an organ-specific response with

415 differential modulation of genes and apocarotenoids in roots *versus* shoots (**Fig. 3, Fig. 4**).

416 In particular, in roots Apo9, OH-Apo9, Apo10 and OH-Apo10 are much more abundant in the

417 MYC samples across almost all the time points analyzed and do not accumulate under +Pi, which

418 suggests that they may be important for the AM colonization process. Apo9 is β-ionone, a cleavage

419 product of several CCD enzymes (CCD1, CCD4, and CCD7) which was shown to have a role in

420 plant-fungal interactions (Wilson *et al.*, 1981; Sharma *et al.*, 2012). However, its specific

421 involvement in the AM symbiosis has not been characterized yet. As in our dataset, CCD7 displays

422 an AM-responsive expression profile and it is involved in SLs biosynthesis, we envisage that β-

423 ionone accumulation in AM roots is mainly due to CCD7 activity. It is worth noting that CCD7

424 could also be involved in the synthesis of blumenol-type metabolites and mycorradicin that

425 accumulate in roots in the late stage of AM colonization (Wang *et al.*, 2018; Fiorilli *et al.*, 2019);

426 we can also hypothesize that β-ionone is a precursor of blumenols. However, due to lack of

427 authentic standards, we were not able to monitor blumenol derivatives.

428 Interestingly, we observed the accumulation at the middle and late stages of mycorrhization of

429 zaxinone and OH-Apo10, which is the precursor of zaxinone, indicating that mycorrhization

430 stimulates multiple steps of this branch of the apocarotenoid biochemical pathway. Notably, the

431 expression of *ZAS1* (and partially *ZAS2*) was also highly influenced by the MYC condition in roots,

432 confirming its correlation with zaxinone (**Fig. 1, Fig. 5**). The association between *CCD8* and *ZAS1*

433 at 7 dpi is in line with previous data showing their interplay at the early stage of the AM symbiosis

434 (Votta *et al.*, 2022).

435 Apo11 level increased at 7 dpi and decreased at 21 dpi, while OH-Apo11 and OH-Apo11 isomers

436 could be associated with the 21 dpi MYC condition. Importantly, the apocarotenoids Apo11 and

437 OH-Apo11 were recently described as being part of an alternative zeaxanthin epoxidase-

438 independent pathway to produce ABA (Jia *et al.*, 2022). Moreover, these compounds act like ABA

439 in maintaining seed dormancy and inducing the expression of ABA-responsive genes (Zheng *et al.*,

440 2021; Jia *et al.*, 2022). In light of these findings, we could hypothesize that Apo11 and OH-Apo11,

441 could be involved in the AM symbiosis, and deserve more investigations along the whole

442 colonization process and in relation to what has been already described for ABA in mycorrhizal

443 roots (López-Ráez *et al.*, 2010; Pozo *et al.*, 2015).

444 The composition of shoot apocarotenoids seems to be most influenced by the time point considered.
445 At 7 dpi, we observe a trend to a decrease of most apocarotenoids, especially in the +Pi compared
446 to -Pi condition. At 21 dpi, the MYC and +Pi conditions showed a similar pattern with a general
447 increase in the level of several apocarotenoids. At 35 dpi, MYC and +Pi conditions again displayed
448 a similar profile, but with a general decrease of several apocarotenoids content. From these
449 observations, it can be speculated that the similarity between the MYC and the +Pi conditions could
450 mirror the Pi nutritional status since the AM symbiosis guarantees an improved Pi mineral nutrition
451 mimicking the high Pi condition (Zouari *et al.*, 2014). Moreover, our data indicate that the OH-
452 Apo11 isomer deserves more investigation as it could be considered a shoot marker of the early
453 stage of AM colonization.
454 We also attempted to associate the expression of specific genes with the accumulation of specific
455 apocarotenoids with a data fusion approach as the genes involved in the production of many
456 apocarotenoids are largely unknown. The reliability of the approach was confirmed by the
457 association between *ZAS1* and zaxinone and its precursor in roots and by the correlation between
458 *CCD7* and β-ionone (**Fig. 5**). In this context, we can speculate that *CCD1* and *CCD4a* are linked to
459 the production of OH-Apo15 and its isomer, since they are correlated in the shoot and both organs,
460 respectively (**Fig. 5**). Interestingly, a fungal *CCD*, *NosACO*, mediates Apo15 (retinal) production
461 (Scherzinger *et al*., 2006), indicating that CCD1/4, or still unidentified CCDs, are involved in
462 Apo15 formation during the AM symbiosis. In addition, the expression of *ZAS1* in shoots is also
463 related to the accumulation of zaxinone, suggesting a direct involvement of this enzyme in
464 endogenous zaxinone level in shoots.
465 In conclusion, our data show the specific profiles of *CCD* genes and apocarotenoids across different
466 stages of the AM symbiosis and Pi conditions, possibly highlighting novel markers at both local and
467 systemic levels. Moreover, this combined approach is a promising tool to further dissect this
468 complex metabolic pathway, suggesting putative links between enzymatic activities and
469 apocarotenoid production.

Supplementary data

Table S1. List of primers used in this study.

Fig. S1. Data-fusion setup.

Fig. S2. Mycorrhization level in rice mycorrhizal plants across a time course (7, 21, and 35 dpi).

Fig. S3. qRT-PCR analysis of transcript levels of CCDs genes in rice root and shoot.

Fig. S4. Principal component analysis (PC1/PC2) of root and shoot CCDs genes across the three growth stages and conditions used in this study.

Fig. S5. Apocarotenoids quantification across the three time points and the three analyzed conditions.

Fig. S6. Plot of the raw apocarotenoids dataset, including the extreme values.

Fig. S7. Principal component analysis (PC1/PC2) of root and shoot apocarotenoids across the three growth stages and conditions used in this study.

Acknowledgements

Author contributions

VF, SA-B, and LL designed and coordinated the investigation. CV and JYW performed the gene expression profiles and carried out the quantification of apocarotenoids with the help from KIL. NC and FS performed the PCA analysis. All authors contributed to the results and discussion. CV, VF, SA-B and LL wrote the article and all the authors contributed to manuscript review & editing.

Conflict of interest

No conflict of interest declared.

Funding

498

Data availability

The data supporting the findings of this study are available within the paper and within its supplementary data published online.

References

Ablazov A, Mi J, Jamil M, Jia K-P, Wang JY, Feng Q, Al-Babili S. 2020. The apocarotenoid zaxinone is a positive regulator of strigolactone and abscisic acid biosynthesis in Arabidopsis roots. Frontiers in Plant Science **11,** 578.

Ablazov A, Votta C, Fiorilli V, *et al.* 2023. ZAXINONE SYNTHASE 2 regulates growth and arbuscular mycorrhizal symbiosis in rice. Plant Physiology **191**, 382–399.

Ahrazem O, Gómez-Gómez L, Rodrigo MJ, Avalos J, Limón MC. 2016. Carotenoid cleavage oxygenases from microbes and photosynthetic organisms: features and functions. International Journal of Molecular Sciences **17**, 1781.

Alder A, Jamil M, Marzorati M, Bruno M, Vermathen M, Bigler P, Ghisla S, Bouwmeester H, Beyer P, Al-Babili S. 2012. The path from β-carotene to carlactone, a strigolactone-like plant hormone. Science **335**, 1348–1351.

Auldridge ME, McCarty DR, Klee HJ. 2006. Plant carotenoid cleavage oxygenases and their apocarotenoid products. Current Opinion in Plant Biology **9**, 315–321.

Bonfante P, Requena N. 2011. Dating in the dark: how roots respond to fungal signals to establish arbuscular mycorrhizal symbiosis. Current Opinion in Plant Biology **14**, 451–457.

Borràs E, Ferré J, Boqué R, Mestres M, Aceña L, Busto O. 2015. Data fusion methodologies for food and beverage authentication and quality assessment A review. Analytica Chimica Acta **891**, 1–14.

Bro R, K. Smilde A. 2014. Principal component analysis. Analytical Methods **6**, 2812–2831.

Brundrett MC. 2009. Mycorrhizal associations and other means of nutrition of vascular plants: understanding the global diversity of host plants by resolving conflicting information and developing reliable means of diagnosis. Plant and Soil **320**, 37–77.

Bruno M, Beyer P, Al-Babili S. 2015. The potato carotenoid cleavage dioxygenase 4 catalyzes a single cleavage of β-ionone ring-containing carotenes and non-epoxidated xanthophylls. Archives of Biochemistry and Biophysics **572**, 126–133.

528 **Bruno M, Koschmieder J, Wuest F, Schaub P, Fehling-Kaschek M, Timmer J, Beyer P, Al-**
529   **Babili S**. 2016. Enzymatic study on AtCCD4 and AtCCD7 and their potential to form
530   acyclic regulatory metabolites. Journal of Experimental Botany **67**, 5993–6005.

531 **Carbonnel S, Gutjahr C**. 2014. Control of arbuscular mycorrhiza development by nutrient signals.
532   Frontiers in Plant Science **5**.

533 **Cazzonelli CI**. 2011. Carotenoids in nature: insights from plants and beyond. Functional Plant
534   Biology **38**, 833.

535 **Charpentier M, Sun J, Wen J, Mysore KS, Oldroyd GED**. 2014. Abscisic acid promotion of
536   arbuscular mycorrhizal colonization requires a component of the PROTEIN
537   PHOSPHATASE 2A complex. Plant Physiology **166**, 2077–2090.

538 **Chen M, Arato M, Borghi L, Nouri E, Reinhardt D**. 2018. Beneficial services of arbuscular
539   mycorrhizal fungi from ecology to application. Frontiers in Plant Science **9**, 1270.

540 **Chen G-TE, Wang JY, Jamil M, Braguy J, Al-Babili S**. 2022. 9-cis-β-Apo-10□-carotenal is the
541   precursor of strigolactones in planta. Planta **256**, 88.

542 **Das D, Paries M, Hobecker K, Gigl M, Dawid C, Lam H-M, Zhang J, Chen M, Gutjahr C**.
543   2022. PHOSPHATE STARVATION RESPONSE transcription factors enable arbuscular
544   mycorrhiza symbiosis. Nature Communications **13**, 477.

545 **Felemban A, Braguy J, Zurbriggen MD, Al-Babili S**. 2019. Apocarotenoids involved in plant
546   development and stress response. Frontiers in Plant Science **10**, 1168.

547 **Fester T, Schmidt D, Lohse S, Walter M, Giuliano G, Bramley P, Fraser P, Hause B, Strack**
548   **D**. 2002. Stimulation of carotenoid metabolism in arbuscular mycorrhizal roots. Planta **216**,
549   148–154.

550 **Fiorilli V, Catoni M, Miozzi L, Novero M, Accotto GP, Lanfranco L**. 2009. Global and cell-type
551   gene expression profiles in tomato plants colonized by an arbuscular mycorrhizal fungus.
552   The New Phytologist **184**, 975–987.

553 **Fiorilli V, Vannini C, Ortolani F, et al.** 2018. Omics approaches revealed how arbuscular
554   mycorrhizal symbiosis enhances yield and resistance to leaf pathogen in wheat. Scientific
555   Reports **8**, 9625.

556   **Fiorilli V, Wang JY, Bonfante P, Lanfranco L, Al-Babili S**. 2019. Apocarotenoids: old and new
557   mediators of the arbuscular mycorrhizal symbiosis. Frontiers in Plant Science **10**, 1186.

558   **Floß DS, Hause B, Lange PR, Küster H, Strack D, Walter MH**. 2008. Knock-down of the MEP
559   pathway isogene 1-deoxy-d-xylulose 5-phosphate synthase 2 inhibits formation of
560   arbuscular mycorrhiza-induced apocarotenoids, and abolishes normal expression of
561   mycorrhiza-specific plant marker genes. The Plant Journal **56**, 86–100.

562   **Floss DS, Levy JG, Levesque-Tremblay V, Pumplin N, Harrison MJ**. 2013. DELLA proteins
563   regulate arbuscule formation in arbuscular mycorrhizal symbiosis. Proceedings of the
564   National Academy of Sciences **110**, E5025–E5034.

565   **Floss DS, Schliemann W, Schmidt J, Strack D, Walter MH**. 2008. RNA interference-mediated
566   repression of MtCCD1 in mycorrhizal roots of *Medicago truncatula* causes accumulation of
567   C27 apocarotenoids, shedding light on the functional role of CCD1. Plant Physiology **148**,
568   1267–1282.

569   **Güimil S, Chang H-S, Zhu T, *et al.*** 2005. Comparative transcriptomics of rice reveals an ancient
570   pattern of response to microbial colonization. Proceedings of the National Academy of
571   Sciences **102**, 8066–8070.

572   **Gutjahr C**. 2014. Phytohormone signaling in arbuscular mycorhiza development. Current Opinion
573   in Plant Biology **20**, 26–34.

574   **Gutjahr C, Parniske M**. 2013. Cell and developmental biology of arbuscular mycorrhiza
575   symbiosis. Annual Review of Cell and Developmental Biology **29**, 593–617.

576   **Haider I, Yunmeng Z, White F, *et al***. 2023. Transcriptome analysis of the phosphate starvation
577   response sheds light on strigolactone biosynthesis in rice. The Plant Journal, published
578   online ahead of print.

579   **Hammer O, Harper DAT, Ryan PD**. 2001. PAST: Paleontological statistics software package for
580   education and data analysis. Palaeontologia Electronica, **4**, 9.

581   **Harrison MJ**. 2012. Cellular programs for arbuscular mycorrhizal symbiosis. Current Opinion in
582   Plant Biology **15**, 691–698.

583 **Harrison PJ, Bugg TDH**. 2014. Enzymology of the carotenoid cleavage dioxygenases: Reaction
584   mechanisms, inhibition and biochemical roles. Archives of Biochemistry and Biophysics
585   **544**, 105–111.

586 **Herrera-Medina MJ, Steinkellner S, Vierheilig H, Ocampo Bote JA, García Garrido JM**.
587   2007. Abscisic acid determines arbuscule development and functionality in the tomato
588   arbuscular mycorrhiza. New Phytologist **175**, 554–564.

589 **Hill EM, Robinson LA, Abdul-Sada A, Vanbergen AJ, Hodge A, Hartley SE**. 2018. Arbuscular
590   mycorrhizal fungi and plant chemical defence: effects of colonisation on aboveground and
591   belowground metabolomes. Journal of Chemical Ecology **44**, 198–208.

592 **Hou X, Rivers J, León P, McQuinn RP, Pogson BJ**. 2016. synthesis and function of
593   apocarotenoid signals in plants. Trends in Plant Science **21**, 792–803.

594 **Huang F-C, Molnár P, Schwab W**. 2009. Cloning and functional characterization of carotenoid
595   cleavage dioxygenase 4 genes. Journal of Experimental Botany **60**, 3011–3022.

596 **Ilg A, Beyer P, Al-Babili S**. 2009. Characterization of the rice carotenoid cleavage dioxygenase 1
597   reveals a novel route for geranial biosynthesis: A novel route for geranial formation. FEBS
598   Journal **276**, 736–747.

599 **Ilg A, Bruno M, Beyer P, Al-Babili S**. 2014. Tomato carotenoid cleavage dioxygenases 1A and
600   1B: Relaxed double bond specificity leads to a plenitude of dialdehydes, mono-
601   apocarotenoids and isoprenoid volatiles. FEBS Open Bio **4**, 584–593.

602 **Jia K-P, Baz L, Al-Babili S**. 2018. From carotenoids to strigolactones. Journal of Experimental
603   Botany **69**, 2189–2204.

604 **Jia K-P, Mi J, Ali S, *et al.*** 2022. An alternative, zeaxanthin epoxidase-independent abscisic acid
605   biosynthetic pathway in plants. Molecular Plant **15**, 151–166.

606 **Klingner A, Bothe H, Wray V, Marner F-J**. 1995. Identification of a yellow pigment formed in
607   maize roots upon mycorrhizal colonization. Phytochemistry **38**, 53–55.

608 **Li Vigni M, Durante C, Cocchi M**. 2013. Chapter 3 Exploratory Data Analysis. In: Marini F, ed.
609   Chemometrics in Food Chemistry. Data Handling in Science and Technology. Elsevier, 55–
610   126.

611 **López-Ráez JA, Charnikhova T, Gómez-Roldán V, *et al.*** 2008. Tomato strigolactones are
612   derived from carotenoids and their biosynthesis is promoted by phosphate starvation. New
613   Phytologist **178**, 863–874.

614 **López-Ráez JA, Kohlen W, Charnikhova T, *et al.*** 2010. Does abscisic acid affect strigolactone
615   biosynthesis? New Phytologist **187**, 343–354.

616 **Ma G, Zhang L, Matsuta A, Matsutani K, Yamawaki K, Yahata M, Wahyudi A, Motohashi
617   R, Kato M**. 2013. Enzymatic Formation of β-Citraurin from β-Cryptoxanthin and
618   Zeaxanthin by Carotenoid Cleavage Dioxygenase4 in the Flavedo of Citrus Fruit. Plant
619   Physiology **163**, 682–695.

620 **MacLean AM, Bravo A, Harrison MJ**. 2017. Plant signaling and metabolic pathways enabling
621   arbuscular mycorrhizal symbiosis. The Plant Cell **29**, 2319–2335.

622 **Maier W, Hammer K, Dammann U, Schulz B, Strack D**. 1997. Accumulation of sesquiterpenoid
623   cyclohexenone derivatives induced by an arbuscular mycorrhizal fungus in members of the
624   Poaceae. Planta **202**, 36–42.

625 **Martín-Rodríguez JA, Huertas R, Ho-Plágaro T, Ocampo JA, Turečková V, Tarkowská D,
626   Ludwig-Müller J, García-Garrido JM**. 2016. Gibberellin–abscisic acid balances during
627   arbuscular mycorrhiza formation in tomato. Frontiers in Plant Science **7**, 1273.

628 **Martín-Rodríguez JÁ, León-Morcillo R, Vierheilig H, Ocampo JA, Ludwig-Müller J, García-
629   Garrido JM**. 2011. Ethylene-dependent/ethylene-independent ABA regulation of tomato
630   plants colonized by arbuscular mycorrhiza fungi. New Phytologist **190**, 193–205.

631 **McQuinn RP, Giovannoni JJ, Pogson BJ**. 2015. More than meets the eye: from carotenoid
632   biosynthesis, to new insights into apocarotenoid signaling. Current Opinion in Plant Biology
633   **27**, 172–179.

634 **Mi J, Al-Babili S**. 2019. To color or to decolor: that is the question. Molecular Plant **12**, 1173–
635   1175.

636 **Mi J, Jia K-P, Wang JY, Al-Babili S**. 2018. A rapid LC-MS method for qualitative and
637   quantitative profiling of plant apocarotenoids. Analytica Chimica Acta **1035**, 87–95.

638 **Moise AR, Al-Babili S, Wurtzel ET**. 2014. Mechanistic aspects of carotenoid biosynthesis.
639   Chemical Reviews **114**, 164–193.

640 **Moreno JC, Mi J, Alagoz Y, Al□Babili S**. 2021. Plant apocarotenoids: from retrograde signaling
641   to interspecific communication. The Plant Journal **105**, 351–375.

642 **Müller LM, Harrison MJ**. 2019. Phytohormones, miRNAs, and peptide signals integrate plant
643   phosphorus status with arbuscular mycorrhizal symbiosis. Current Opinion in Plant Biology
644   **50**, 132–139.

645 **Nadal M, Paszkowski U**. 2013. Polyphony in the rhizosphere: presymbiotic communication in
646   arbuscular mycorrhizal symbiosis. Current Opinion in Plant Biology **16**, 473–479.

647 **Nambara E, Marion-Poll A**. 2005. Abscisic acid biosynthesis and catabolism. Annual Review of
648   Plant Biology **56**, 165–185.

649 **Nisar N, Li L, Lu S, Khin NC, Pogson BJ**. 2015. Carotenoid metabolism in plants. Molecular
650   Plant **8**, 68–82.

651 **Pozo MJ, Jung SC, López-Ráez JA, Azcón-Aguilar C**. 2010. Impact of Arbuscular Mycorrhizal
652   Symbiosis on Plant Response to Biotic Stress: The Role of Plant Defence Mechanisms. In:
653   Koltai H,, In: Kapulnik Y, eds. Arbuscular Mycorrhizas: Physiology and Function.
654   Dordrecht: Springer Netherlands, 193–207.

655 **Pozo MJ, López-Ráez JA, Azcón-Aguilar C, García-Garrido JM**. 2015. Phytohormones as
656   integrators of environmental signals in the regulation of mycorrhizal symbioses. New
657   Phytologist **205**, 1431–1436.

658 **Richardson AE, Lynch JP, Ryan PR,** *et al.* 2011. Plant and microbial strategies to improve the
659   phosphorus efficiency of agriculture. Plant and Soil **349**, 121–156.

660 **Rodrigo MJ, Alquézar B, Alós E, Medina V, Carmona L, Bruno M, Al-Babili S, Zacarías L**.
661   2013. A novel carotenoid cleavage activity involved in the biosynthesis of *Citrus* fruit-
662   specific apocarotenoid pigments. Journal of Experimental Botany **64**, 4461–4478.

663 **Scannerini S, Bonfante-Fasolo P**. 1977. Unusual plasties in an endomycorrhizal root. Canadian
664   Journal of Botany **55**, 2471–2474.

665 **Scherzinger D, Ruch S, Kloer DP, Wilde A, Al-Babili S**. 2006. Retinal is formed from apo-
666   carotenoids in *Nostoc* sp. PCC7120: *in vitro* characterization of an apo-carotenoid
667   oxygenase. Biochemical Journal **15**;398(3):361-9.

668 **Schwartz SH, Qin X, Zeevaart JD**. 2001. Characterization of a novel carotenoid cleavage
669   dioxygenase from plants. Journal of Biological Chemistry **276**, 25208–25211.

670 **Sharma V, Singh G, Kaur H, Saxena AK, Ishar MPS**. 2012. Synthesis of β-ionone derived
671   chalcones as potent antimicrobial agents. Bioorganic & Medicinal Chemistry Letters **22**,
672   6343–6346.

673 **Shi J, Zhao B, Zheng S, *et al.*** 2021. A phosphate starvation response-centered network regulates
674   mycorrhizal symbiosis. Cell **184**, 5527-5540.e18.

675 **Smith SE, Jakobsen I, Grønlund M, Smith FA**. 2011. Roles of arbuscular mycorrhizas in plant
676   phosphorus nutrition: interactions between pathways of phosphorus uptake in arbuscular
677   mycorrhizal roots have important implications for understanding and manipulating plant
678   phosphorus acquisition. Plant Physiology **156**, 1050–1057.

679 **Spatafora JW, Chang Y, Benny GL, *et al.*** 2016. A phylum-level phylogenetic classification of
680   zygomycete fungi based on genome-scale data. Mycologia **108**, 1028–1046.

681 **Strack D, Fester T**. 2006. Isoprenoid metabolism and plastid reorganization in arbuscular
682   mycorrhizal roots. New Phytologist **172**, 22–34.

683 **Sui X, Kiser PD, Lintig J von, Palczewski K**. 2013. Structural basis of carotenoid cleavage: From
684   bacteria to mammals. Archives of Biochemistry and Biophysics **539**, 203–213.

685 **Tan B-C, Joseph LM, Deng W-T, Liu L, Li Q-B, Cline K, McCarty DR**. 2003. Molecular
686   characterization of the *Arabidopsis* 9-*cis* epoxycarotenoid dioxygenase gene family. The
687   Plant Journal: For Cell and Molecular Biology **35**, 44–56.

688 **Vogel JT, Tan B-C, McCarty DR, Klee HJ**. 2008. The carotenoid cleavage dioxygenase 1
689   enzyme has broad substrate specificity, cleaving multiple carotenoids at two different bond
690   positions. Journal of Biological Chemistry **283**, 11364–11373.

691 **Volpe V, Chialva M, Mazzarella T, Crosino A, Capitanio S, Costamagna L, Kohlen W, Genre
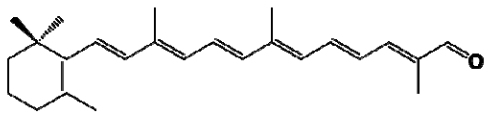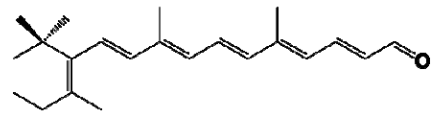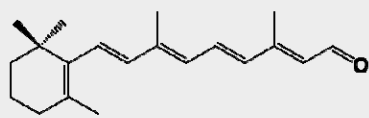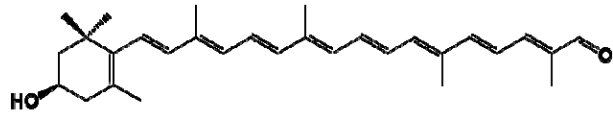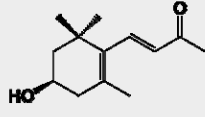692   A**. Long-lasting impact of chitooligosaccharide application on strigolactone biosynthesis
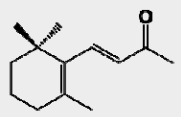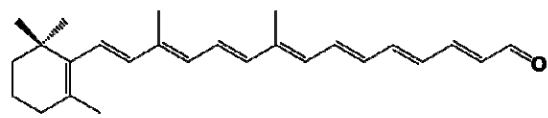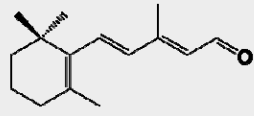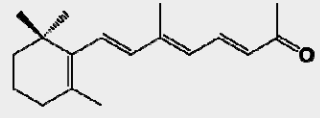
693 and fungal accommodation promotes arbuscular mycorrhiza in *Medicago truncatula*. New
694 Phytologist **237**:2316–2331.

695 **Votta C, Fiorilli V, Haider I,** *et al.* 2022. Zaxinone synthase controls arbuscular mycorrhizal
696 colonization level in rice. The Plant Journal **111**, 1688–1700.

697 **Walter MH, Fester T, Strack D**. 2000. Arbuscular mycorrhizal fungi induce the non-mevalonate
698 methylerythritol phosphate pathway of isoprenoid biosynthesis correlated with accumulation
699 of the 'yellow pigment' and other apocarotenoids: Mycorrhizal induction of isoprenoid
700 biosynthesis. The Plant Journal **21**, 571–578.

701 **Walter MH, Floß DS, Hans J, Fester T, Strack D**. 2007. Apocarotenoid biosynthesis in
702 arbuscular mycorrhizal roots: Contributions from methylerythritol phosphate pathway
703 isogenes and tools for its manipulation. Phytochemistry **68**, 130–138.

704 **Walter MH, Floss DS, Strack D**. 2010. Apocarotenoids: hormones, mycorrhizal metabolites and
705 aroma volatiles. Planta **232**, 1–17.

706 **Wang JY, Chen G-TE, Jamil M, Braguy J, Sioud S, Liew KX, Balakrishna A, Al-Babili S**.
707 2022. Protocol for characterizing strigolactones released by plant roots. STAR Protocols **3**,
708 101352.

709 **Wang JY, Haider I, Jamil M,** *et al.* 2019. The apocarotenoid metabolite zaxinone regulates
710 growth and strigolactone biosynthesis in rice. Nature Communications **10**, 810.

711 **Wang JY, Lin P-Y, Al-Babili S**. 2021. On the biosynthesis and evolution of apocarotenoid plant
712 growth regulators. Seminars in Cell & Developmental Biology **109**, 3–11.

713 **Wang B, Qiu Y-L**. 2006. Phylogenetic distribution and evolution of mycorrhizas in land plants.
714 Mycorrhiza **16**, 299–363.

715 **Wang W, Shi J, Xie Q, Jiang Y, Yu N, Wang E**. 2017. Nutrient exchange and regulation in
716 arbuscular mycorrhizal symbiosis. Molecular Plant **10**, 1147–1158.

717 **Wang Y, Wang M, Li Y, Wu A, Huang J**. 2018. Effects of arbuscular mycorrhizal fungi on
718 growth and nitrogen uptake of *Chrysanthemum morifolium* under salt stress (L-SP Tran,
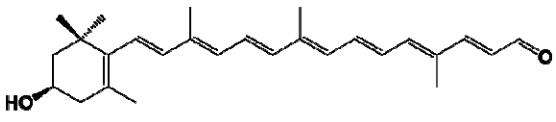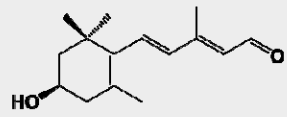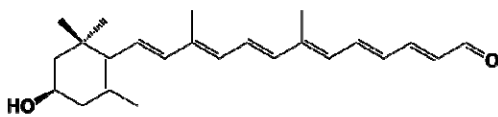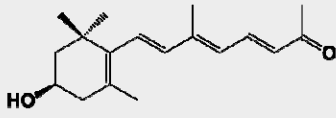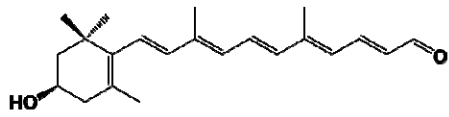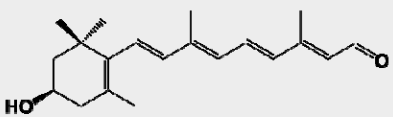719 Ed.). PLOS ONE **13**, e0196408.

720 **Waters MT, Gutjahr C, Bennett T, Nelson DC**. 2017. Strigolactone *Signaling and Evolution*.
721   Annual Review of Plant Biology **68**, 291–322.

722 **Wilson DM, Gueldner RC, Mckinney JK, Lievsay RH, Evans BD, Hill RA**. 1981. Effect of *β*-
723   Ionone on *Aspergillus flavus* and *Aspergillus parasiticus* growth, sporulation, morphology
724   and aflatoxin production. Journal of the American Oil Chemists' Society **58**, A959–A961.

725 **Yoneyama K, Kisugi T, Xie X, Yoneyama K**. 2013. Chemistry of strigolactones: why and how do
726   plants produce so many strigolactones? Molecular Microbial Ecology of the Rhizosphere.
727   John Wiley & Sons, Ltd, 373–379.

728 **Yoneyama K, Xie X, Kusumoto D, Sekimoto H, Sugimoto Y, Takeuchi Y, Yoneyama K**. 2007.
729   Nitrogen deficiency as well as phosphorus deficiency in sorghum promotes the production
730   and exudation of 5-deoxystrigol, the host recognition signal for arbuscular mycorrhizal
731   fungi and root parasites. Planta **227**, 125–132.

732 **Zheng X, Mi J, Balakrishna A, Liew KX, Ablazov A, Sougrat R, Al-Babili S**. 2022. *Gardenia*
733   carotenoid cleavage dioxygenase 4a is an efficient tool for biotechnological production of
734   crocins in green and non-green plant tissues. Plant Biotechnology Journal **20**, 2202–2216.

735 **Zheng X, Yang Y, Al-Babili S**. 2021. Exploring the diversity and regulation of apocarotenoid
736   metabolic pathways in plants. Frontiers in Plant Science **12**, 787049.

737 **Zouari I, Salvioli A, Chialva M, Novero M, Miozzi L, Tenore GC, Bagnaresi P, Bonfante P**.
738   2014. From root to fruit: RNA-Seq analysis shows that arbuscular mycorrhizal symbiosis
739   may affect tomato fruit metabolism. BMC Genomics **15**, 221.

740 **Tables**

741 Table 1. A summary with non-hydroxylated and hydroxylated apocarotenoids analyzed in this

742 study, the formula, corresponding name, and structural formula are indicated for each abbreviation.

Abbreviation	Name	Formula	Structural formula
Apo9	β-apo-9'-carotenal (β-ionone)	$C_{13}H_{20}O$	
Apo10	β-apo-10'-carotenal	$C_{27}H_{36}O$	
Apo11	β-apo-11-carotenal	$C_{15}H_{22}O$	
Apo12	β-apo-12'-carotenal	$C_{25}H_{34}O$	
Apo13	β-apo-13-carotenone	$C_{18}H_{26}O$	
Apo14	β-apo-14'-carotenal	$C_{22}H_{30}O$	
Apo15	β-apo-15-carotenal	$C_{20}H_{28}O$	
OH-Apo8	3-OH-β-apo-8'-carotenal	$C_{30}H_{40}O_2$	
OH-Apo9	3-OH-β-apo-8'-carotenal (OH- β-ionone)	$C_{13}H_{20}O_2$	

OH-Apo10	3-OH-β-apo-10'-carotenal	$C_{27}H_{36}O_2$	
OH-Apo11	3-OH-β-apo-11-carotenal	$C_{15}H_{22}O_2$	
OH-Apo12	3-OH-β-apo-12'-carotenal	$C_{25}H_{34}O_2$	
OH-Apo13	3-OH-β-apo-13-carotenone (zaxinone)	$C_{18}H_{26}O_2$	
OH-Apo14	3-OH-β-apo-14'-carotenal	$C_{22}H_{30}O_2$	
OH-Apo15	3-OH-β-apo-15-carotenal	$C_{20}H_{28}O_2$	

743

Figure legends

Fig. 1. Heatmap of root (A) and shoot (B) gene expression of the three-time points (7, 21, 35 dpi: days post inoculation) and the three analyzed conditions (-Pi, MYC, +Pi). Data are means ± SE (n<=4). For each gene and time point, the value of the corresponding -Pi sample was set to 1. Asterisks indicate statistically significant differences referred to the –Pi condition, separately for each time point, by one way-Anova (*P < 0.05; **P<0.01; ***P<0.001). The circles represented the different stages of mycorrhization: at the early stage (7 dpi), the fungus structures, hyphopodia, adhered to the root epidermis, during the middle stage (21 dpi), the arbuscules started their development that will be completed at the later stage (35 dpi). Heatmaps were generated with the MultiExperiment Viewer (MeV) software.

-Pi: 3.2 µM Pi; myc: mycorrhizal plants grown at 3.2 µM Pi; +Pi: 500 µM Pi.

Fig. 2. Principal component analysis of root and shoot CCDs genes expression across the three-time points and the three growth conditions (-P, MYC, +P). Loading plot (A) and scores plot (B) with the third and fifth principal components. In the scores plot (B) for both groups the lines connecting each sample lead to the cluster center.

Fig. 3. Heatmap of root (A) and shoot (B) apocarotenoids quantification across the three time points and the three analyzed conditions (-P, MYC, +P). For each APOs and time point, the value of the corresponding -Pi was set to 1. Data are means ± SE (n<=4). Asterisks indicate statistically significant differences as compared to –P condition, separately for each time point, by one way-Anova (*P < 0.05; **P<0.01; ***P<0.001). The circles represented the different stages of mycorrhization: at the early stage (7 dpi), the fungus structures, called hyphopodia, adhered to the root epidermis, during the middle stage (21 dpi), the arbuscules started their development that will be completed at the later stage (35 dpi). The apocarotenoids indicated with asterisks represented the isoform of the corresponding apocarotenoid. Heatmaps were generated with the MultiExperiment Viewer (MeV) software.

Fig. 4. Principal component analysis of root and shoot APOs across the three growth stages and conditions (-P, MYC, +P). Loading plot (A) and scores plot (B) with the second and third principal components. In the scores plot (B) for both groups the lines connecting each sample lead to the cluster center.

Figure 5. Principal component analysis of root and shoot genes and apocarotenoids datasets fused and analyzed across the three time points and growth conditions (-P, MYC, +P). Loading plot (A) and scores plot (B) with the first and second principal components.
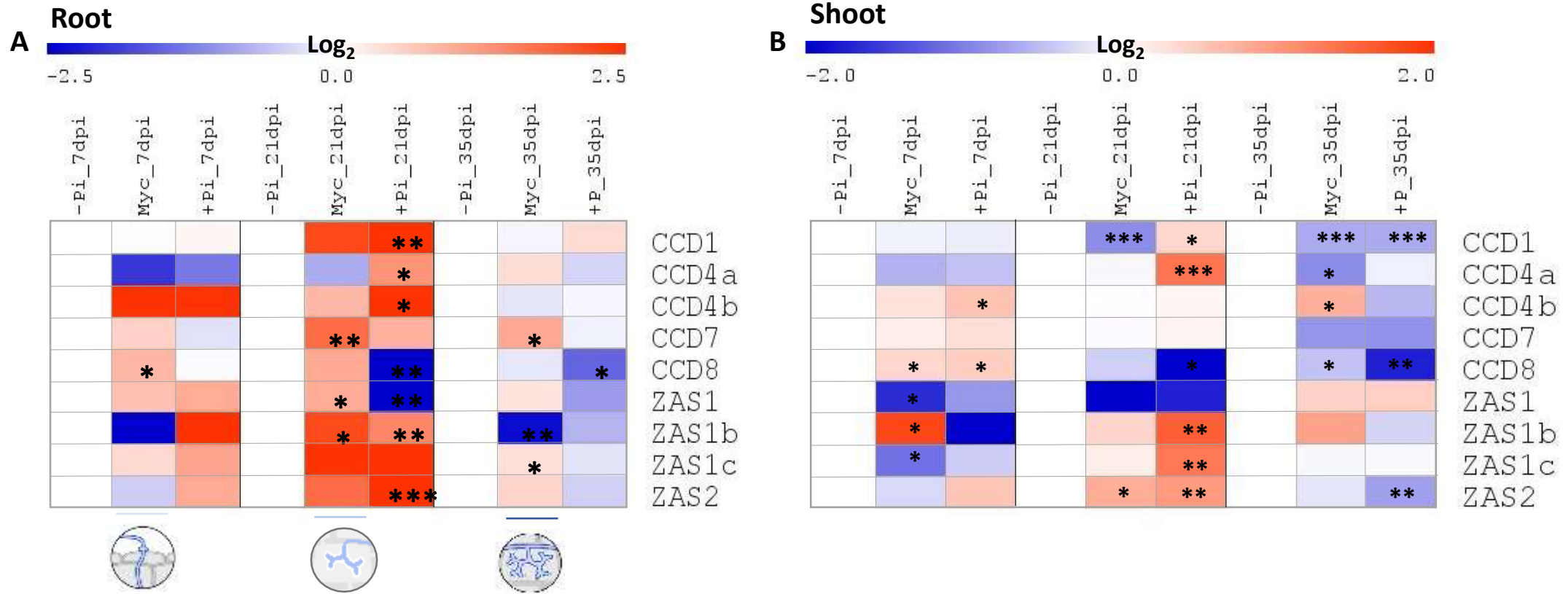
29

Figure 1. *Heatmap of root (A) and shoot (B) gene expression of the three-time points (7, 21, 35 dpi: days post inoculation) and the three analyzed conditions (-Pi, MYC, +Pi). Data are means ± SE (n<=4). For each gene and time point, the value of the corresponding -Pi sample was set to 1. Asterisks indicate statistically significant differences referred to the –Pi condition, separately for each time point, by one way-Anova (*P < 0.05; **P<0.01; ***P<0.001). The circles represented the different stages of mycorrhization: at the early stage (7 dpi), the fungus structures, hyphopodia, adhered to the root epidermis, during the middle stage (21 dpi), the arbuscules started their development that will be completed at the later stage (35 dpi). Heatmaps were generated with the MultiExperiment Viewer (MeV) software.*
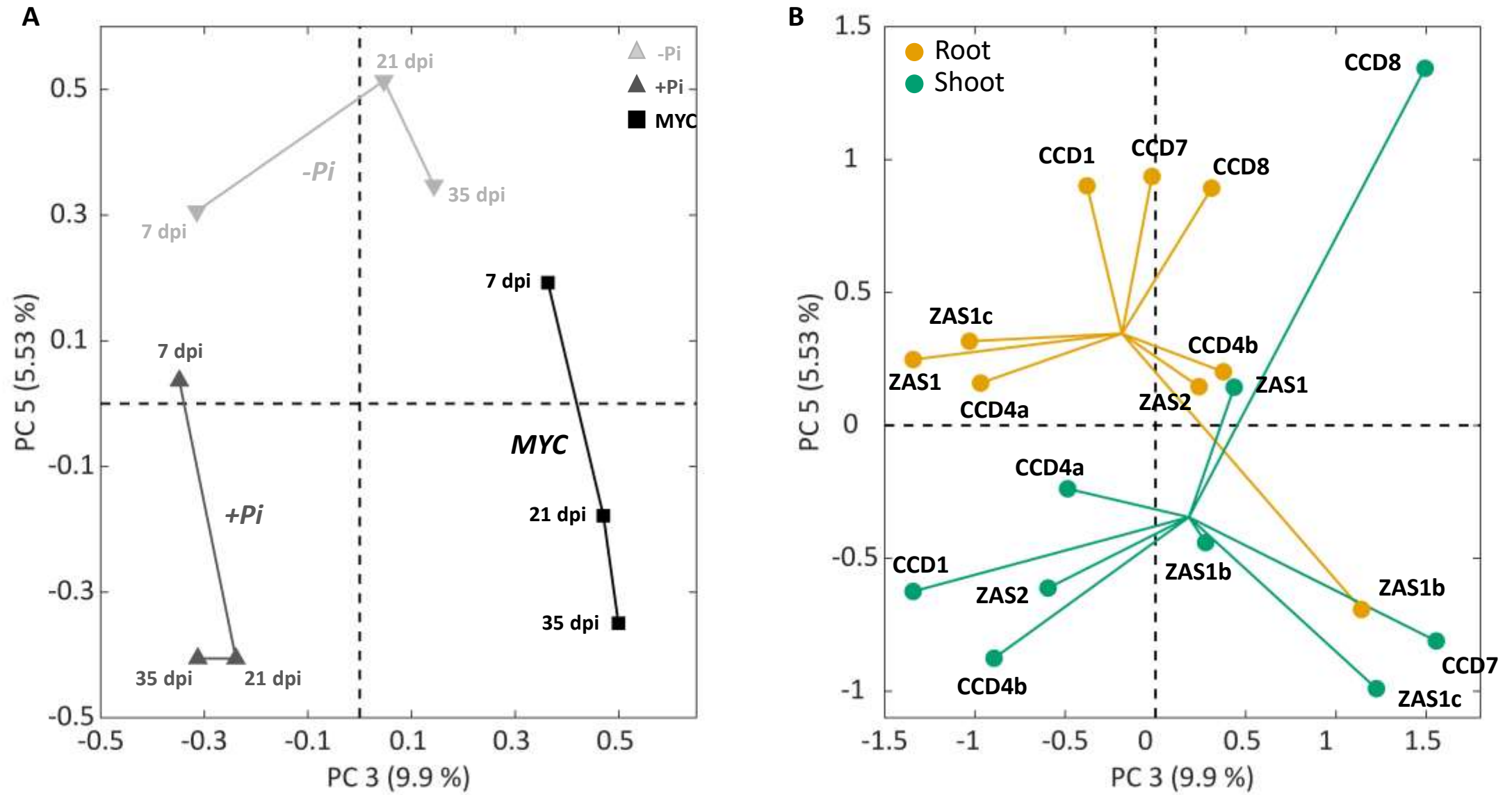*-Pi: 3.2 µM Pi; myc: mycorrhizal plants grown at 3.2 µM Pi; +Pi:500 µM Pi.*

Figure 2. *Principal component analysis of root and shoot CCDs genes expression across the three-time points and the three growth conditions (-Pi, MYC, +Pi). Loadings plot (A) and scores plot (B) show the third and fifth principal components. In the scores plot (B) for both groups the lines connecting each sample lead to the cluster center.*
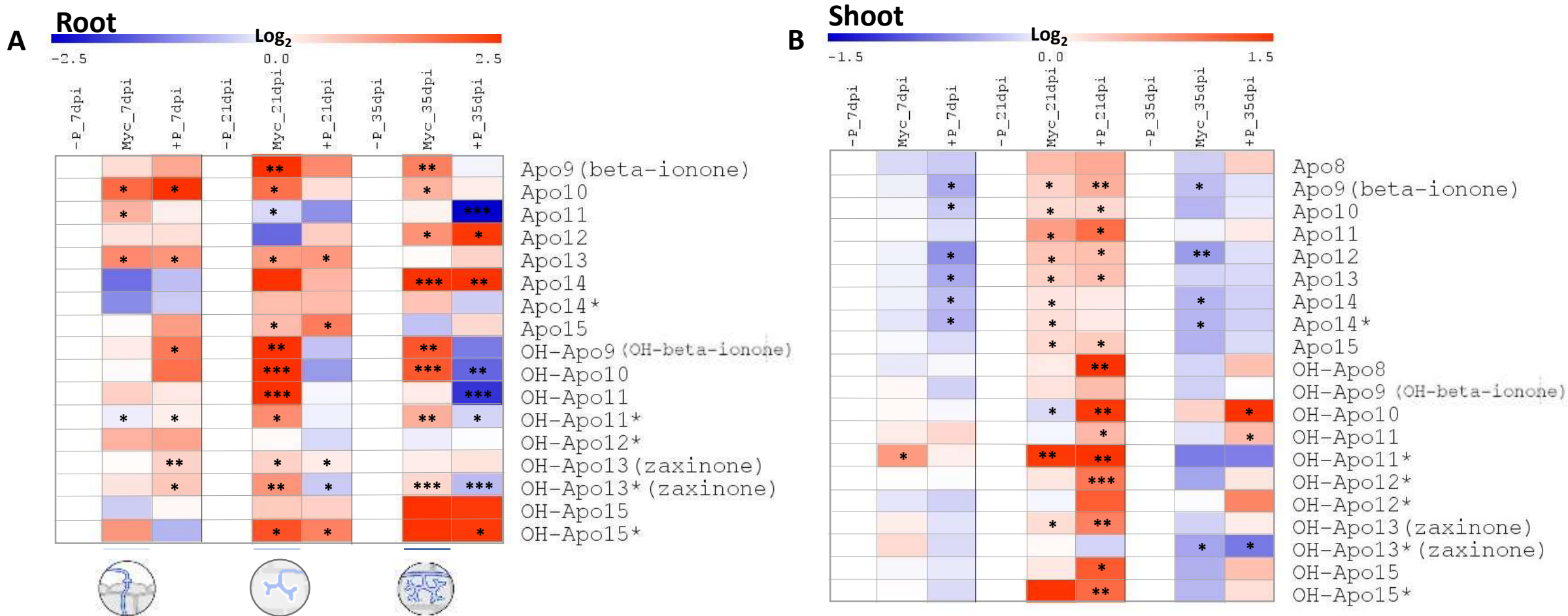
Figure 3. Heatmap of root (A) and shoot (B) apocarotenoids quantification across the three time points and the three analyzed conditions (-P, MYC, +P). For each APOs and time point, the value of the corresponding -Pi was set to 1. Data are means ± SE (n<=4). Asterisks indicate statistically significant differences as compared to –P condition, separately for each time point, by one way-Anova (*P < 0.05; **P<0.01; ***P<0.001). The circles represented the different stages of mycorrhization: at the early stage (7 dpi), the fungus structures, called hyphopodia, adhered to the root epidermis, during the middle stage (21 dpi), the arbuscules started their development that will be completed at the later stage (35 dpi). The apocarotenoids indicated with asterisks represented the isoform of the corresponding apocarotenoid. Heatmaps were generated with the MultiExperiment Viewer (MeV) software.
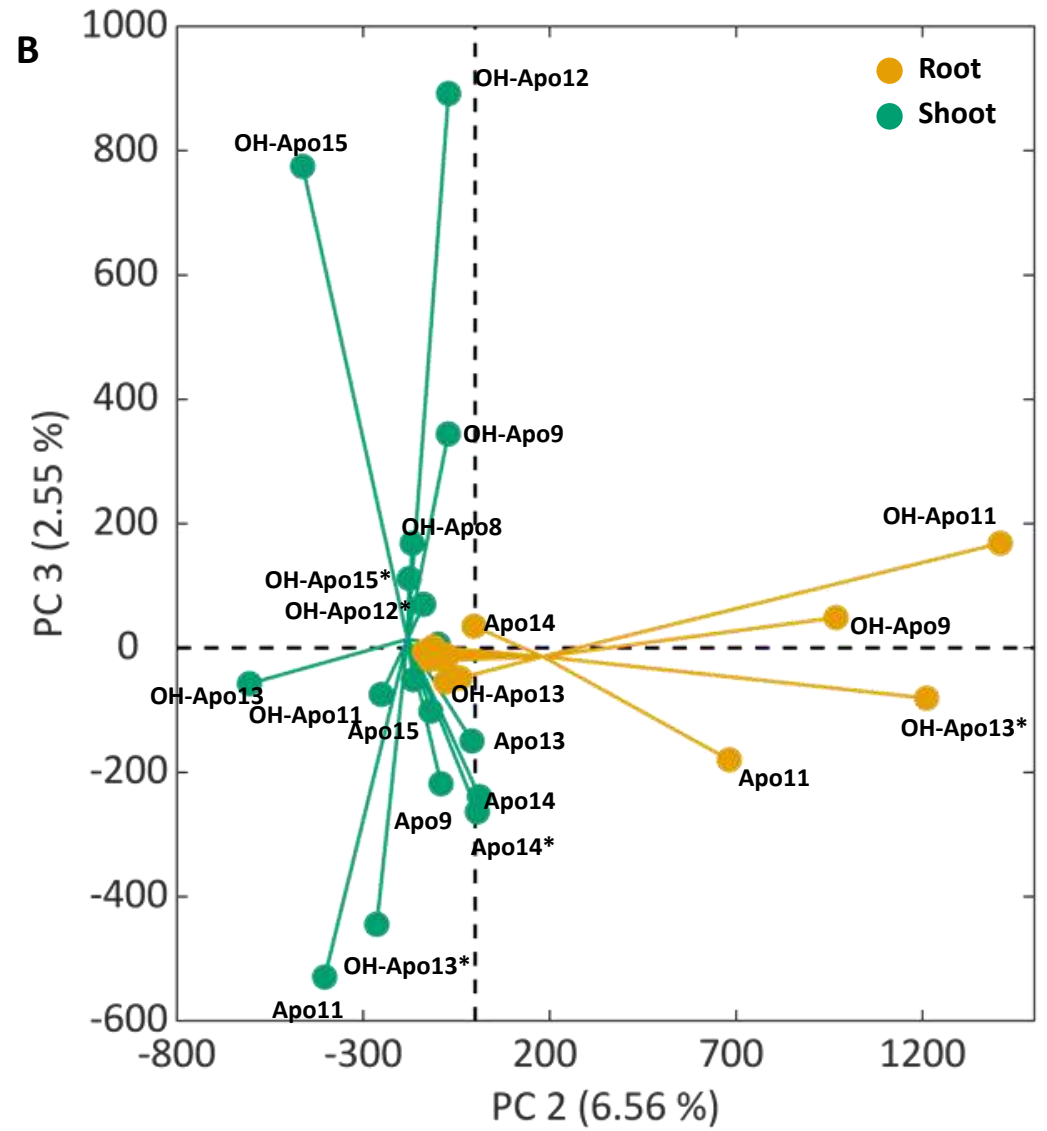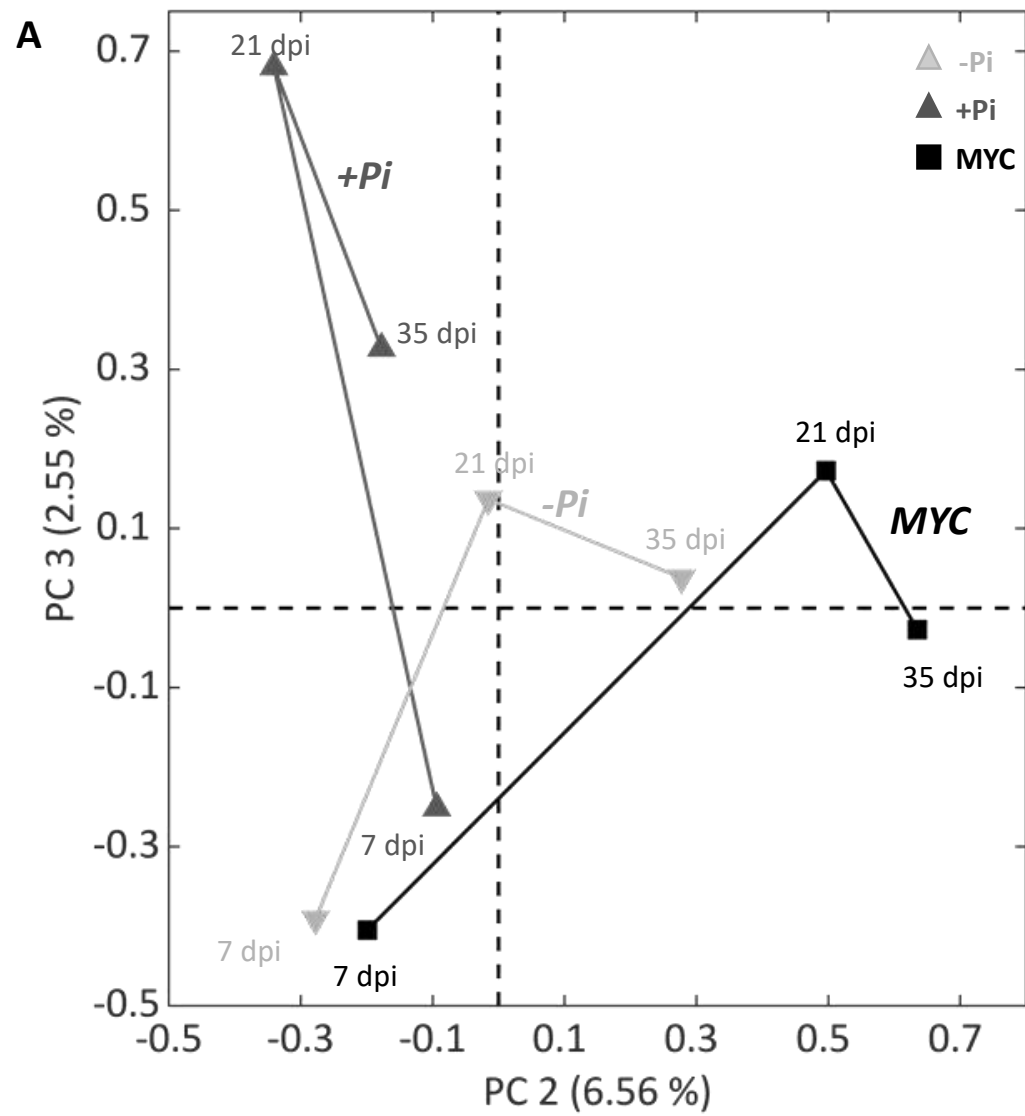
Figure 4. *Principal component analysis of root and shoot APOs across the three-time points and the three growth conditions (-Pi, MYC, +Pi). Loadings plot (A) and scores plot (B) show the second and third principal components. In the scores plot (B) for both groups the lines connecting each sample lead to the cluster center.*
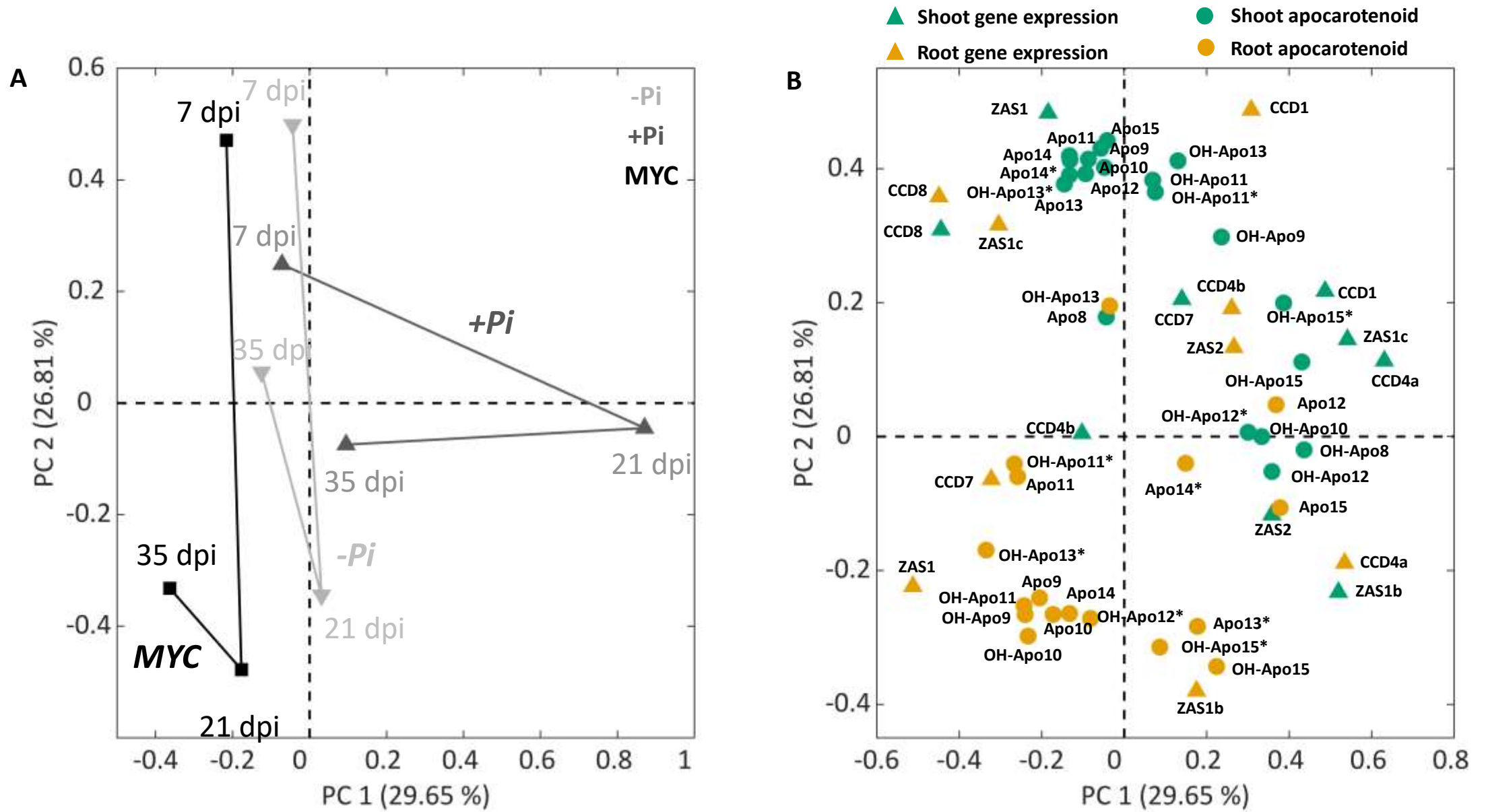
Figure 5. *Principal component analysis of root and shoot genes and apocarotenoids datasets fused and analysed across the three-time points and the three growth conditions (-Pi, MYC, +Pi). Loadings plot (A) and scores plot (B) show the first and second principal components. The apocarotenoids indicated with asterisks represent the isoform of the corresponding apocarotenoid.*